Clim Dyn
DOI 10.1007/s00382-015-2890-9

Simulated sensitivity of the tropical climate to extratropical thermal forcing: tropical SSTs and African land surface

Stefanie Talento[1] · **Marcelo Barreiro**[1]

Received: 10 October 2014 / Accepted: 23 October 2015

Abstract This study investigates the Intertropical Convergence Zone (ITCZ) response to extratropical thermal forcing applied to an atmospheric general circulation model coupled to slab ocean and land models. We focus on the relative roles of the atmosphere, tropical sea surface temperatures (SSTs) and continental surface temperatures in the ITCZ response to the imposed forcing. The forcing consists of cooling in one hemisphere and warming in the other poleward of 40°, with zero global average. Three sets of experiments are performed: in the first the slab ocean and land models are applied globally; in the second the tropical SSTs are kept fixed while the slab land model is applied globally; in the third, in addition, surface temperatures over Africa are kept fixed. Realistic boundary surface conditions are used. We find that the ITCZ shifts towards the warmer hemisphere and that the stronger the forcing, the larger the shift. When the constraint of fixed tropical SST is imposed we find that the ITCZ response is strongly weakened, but it is still not negligible in particular over the Atlantic Ocean and Africa where the precipitation anomalies are of the order of 20 and 60 %, respectively, of the magnitude obtained without the SST restriction. Finally, when the constraint of the African surface temperature is incorporated we find that the ITCZ response completely vanishes, indicating that the ITCZ response to the extratropical forcing is not possible just trough purely atmospheric processes, but needs the involvement of either the tropical SST or the continental surface temperatures. The clear-sky longwave radiation feedback is highlighted as the main physical mechanism operating behind the land-based extratropical to tropical communication.

Keywords ITCZ shift · Extratropical forcing · Tropical sea surface temperatures · Land surface temperature

1 Introduction

Paleoclimatic studies and twentieth century observations suggest that the extratropics have the capability to affect the tropical climate through the development of, both, atmospheric and oceanic teleconnections.

Paleoclimatic studies indicate that, for example, the marine Inter Tropical Convergence Zone (ITCZ) in the eastern Pacific Ocean shifts toward the south when the Northern Hemisphere (NH) is cooled by ice during maximal covering in glacial periods (Lynch-Stieglitz 2004). In addition, evidence obtained in the Cariaco basin in the Caribbean Sea shows that changes in this region might be strongly correlated with high latitude climate, during the last glacial period and Holocene (Peterson et al. 2000; Hughen et al. 2000). Meanwhile, Wang et al. (2004) analyse records of the last 210 kyrs and find that wet periods in northeast Brazil, associated with a southward displacement of the ITCZ, may be synchronized with cold periods in Greenland and Heinrich events in the North Atlantic.

Regarding the twentieth century climate, Folland et al. (1986) found that a sea surface temperature (SST) pattern characterized by an inter-hemispheric thermal gradient could be a possible driver to decadal droughts in the Sahel region and Giannini et al. (2003) were able to reproduce the Sahel precipitation variability prescribing the observed twentieth century SST to an AGCM, In particular, a

✉ Stefanie Talento
stalento@fisica.edu.uy

[1] Department of Atmospheric Sciencies, Institute of Physics, School of Sciences, Universidad de la República, Iguá 4225, 11400 Montevideo, Uruguay

Published online: 04 November 2015

configuration of a cooler NH and a warmer Southern Hemisphere (SH) was associated with a period of Sahel drought starting in the late 1960s.

At the same time, numerical studies show that the tropical climate can be affected in several ways by anomalous conditions in the extratropics: abrupt descent of salinity in the North Atlantic, warming of surface oceanic waters in high latitudes, changes in clouds in high latitudes or extratropical thermal forcings.

The tropical effect of abrupt descents of salinity in the North Atlantic has been studied with focus on two aspects of the ocean dynamics: the thermohaline circulation (Manabe and Stouffer 1995; Rahmstorf 1995; Vellinga and Woods 2002; Stouffer et al. 2006) and the wind-driven circulation (Gu and Philander 1997; Boccaletti et al. 2004; Sun et al. 2004; Barreiro et al. 2008). Both circulations weaken in response to a decrease in the salinity levels and, as a consequence, there is a decrease in the heat transport toward the north as well as an ITCZ displacement to the SH.

The impact of increased SSTs in high latitudes has been analysed, for example, by Liu and Yang (2003) and Yang and Liu (2005). These authors find that the tropical SST response corresponds with half of the SST change imposed in the extratropical forcing region. In addition, they propose that the impact over the tropical SST is obtained through contributions from both the atmosphere and the ocean, being the contributions 70 and 30 %, respectively. On the other hand, they suggest that the main influence comes from the SH, where the ocean/land proportion is higher.

Barreiro and Philander (2008) analyse the impact of the reduction of cloud cover in high latitudes. They conclude that such a change in the planetary albedo can lead to an extratropical and tropical warming and that the cold tongues in the Pacific and Atlantic oceans are weakened. They highlight that the temporal scale for the adjustment to the perturbation in the tropical Pacific can be considered in the range of rapid climate change, as it is of decades to centuries. Furthermore, Burls and Fedorov (2014) deepen on the idea that extratropical cloud cover can have an impact in the tropical regions and demonstrate that there is a near-linear relationship between the meridional gradient in cloud albedo between the tropics and mid-latitudes and the mean zonal SST gradient in the equatorial Pacific.

There are several works highlighting the impact an extratropical thermal forcing (materialized either by changes in the ice cover or by imposed heat fluxes) may have on the tropical climate. Simulations with either atmospheric or coupled models, in aquaplanet mode or with realistic surface boundary conditions, have all shown to shift the position of the ITCZ to the anomalously warm hemisphere.

Chiang and Bitz (2005) study the high latitude imposed ice influence on the marine ITCZ in an atmospheric general circulation model (AGCM) coupled to a slab ocean model. They find that the ITCZ shifts in all the basins meridionally away from the hemisphere with the imposed ice cover. They propose that the imposed cooling is communicated to the tropics by a subtropical Wind-Evaporation-SST (WES) feedback: the anomalous ice induces a cooling and drying of the air and surface over high and mid latitudes, further progression of the cold anomalies occur in the Pacific and Atlantic northeasterly trade wind regions, where the WES feedback initiates progression of the cold SST to the tropical region.

Kang et al. (2008, 2009) study the response of the ITCZ to an antisymmetric inter-hemispheric heat flux with zero global average, in an AGCM coupled to a slab ocean model in aquaplanet mode. They conclude that the ITCZ shifts toward the warmer hemisphere, that the magnitude of the shift increases with the amplitude of the forcing and that the tropical behaviour could be strongly dependent on the model convection scheme and cloud feedbacks. In particular, Kang et al. (2009) showed that the WES feedback is not fundamental as they performed simulations without this feedback and the ITCZ is still displaced to the warmer hemisphere. Schneider et al. (2014) build upon these studies analyzing the ITCZ displacements from an energy flux perspective, and find an anticorrelation between the latitude of the ITCZ and the cross-equatorial atmospheric energy transport.

Recently, Cvijanovic and Chiang (2013) analyse the ITCZ response to a North Atlantic high latitude cooling applied to an AGCM coupled to a slab ocean, using realistic surface boundary conditions focusing on the relative roles of tropical SST and energy flux changes (see also Chiang and Friedman 2012). They argue that the ITCZ shifts are not possible without the tropical SST changes, therefore suggesting that the tropical SSTs are a more suitable driver of tropical precipitation shifts than the atmospheric energy fluxes.

In this study we examine the ITCZ response to an extratropical thermal forcing applied to an AGCM coupled to slab ocean and land models. In comparison with previous studies our simulations are performed with realistic surface boundary conditions, the extratropical forcing pattern consists of warming in one hemisphere and cooling in the other with zero global mean and the effect of the intensity of the forcing is investigated. In that sense this work can be seen as a continuation of that of Cvijanovic and Chiang (2013). Furthermore, the relative roles played by the atmosphere, the tropical SSTs and the continental surface temperatures in the ITCZ response are investigated in a series of experiments designed to separate these influences. In the first series the slab ocean and land models are applied globally. In the second series, the tropical SST role is investigated through simulations in which the slab land

model is applied globally while in the ocean the tropical SSTs are maintained fixed, applying the slab ocean model elsewhere. In this second series we will show that the ITCZ response does not completely vanish if the tropical SSTs are not allowed to change, in particular, over Africa and the Atlantic Ocean. This motivates the third series of experiments in which the role of the surface temperature over Africa is analysed by incorporating the constraint of fixed continental surface temperature over that continent. As will be shown, the role of the African land surface temperature is essential for maintaining the ITCZ response when the tropical SSTs are fixed and, therefore, the last part of this paper investigates the physical mechanisms connecting the extratropical signal to the continental surface temperatures over Africa, via a last experiment in which the clear-sky longwave radiation process is switched off.

The manuscript is organized as follows: in Sect. 2 we introduce the model and the experiments. Results are presented in Sects. 3, 4, 5 and 6. In Sect. 3 we present the experiments where the slab ocean and land models are applied globally. In Sect. 4 we analyse the role of the tropical SST. In Sect. 5 the role of the African surface temperature is studied, while the physical mechanisms connecting the extratropical signal with the African surface temperatures are discussed in Sect. 6. Finally, in Sect. 7 we summarize the conclusions.

2 Model and experiments

The model used in this study is the Abdus Salam International Centre for Theoretical Physics (ICTP) AGCM (Molteni 2003; Kucharski et al. 2006), which is a full atmospheric model with simplified physics. We use the model in its 8-layer configuration and T30 (3.75° × 3.75°) horizontal resolution. Over ocean and land slab models are coupled. Present-day boundary surface conditions, orbital parameters and greenhouse forcing are used. In addition, a monthly-varying ocean heat flux correction is imposed in order to keep the simulated SST close to present-day conditions.

We design experiments in order to study the response of the ITCZ to extratropical thermal forcing, considering increasing intensity of the forcing.

The applied forcing pattern consists in cooling in one hemisphere and warming in the other poleward of 40°, applied only over ocean grid points, and with a resulting global average forcing equal to zero. This pattern is similar to the one used in Kang et al. (2008) and it is intended to represent the asymmetric temperature changes associated with glacial-interglacial and millennial-scale climate variability. The forcing pattern is superposed to a background state and is obtained as explained in the following paragraphs.

Let θ denote latitude, ψ longitude and lsm the land surface mask i.e. lsm = 1 over land, lsm = 0 over sea.

Consider h to be:

$$h(\theta,\psi) = -A\sin\left(\frac{\theta+40}{50}\pi\right) * (1 - lsm(\theta,\psi)) \quad \text{for } \theta \in [-90,-40]$$

$$h(\theta,\psi) = 0 \quad \text{for } \theta \in [-40,40]$$

$$h(\theta,\psi) = -A\sin\left(\frac{\theta-40}{50}\pi\right) * (1 - lsm(\theta,\psi)) \quad \text{for } \theta \in [40,90]$$

where A (W/m^2) denotes the intensity of the forcing.

Then, let h_{SH} and h_{NH} be the integral of h over the *SH* and *NH*, respectively:

$$h_{SH} = \int_{\psi=0}^{\psi=2\pi}\int_{\theta=-\pi/2}^{\theta=0} h(\theta,\psi)d\theta d\psi$$

$$h_{NH} = \int_{\psi=0}^{\psi=2\pi}\int_{\theta=0}^{\theta=\pi/2} h(\theta,\psi)d\theta d\psi$$

Finally, the applied forcing pattern H is defined as:

$$H(\theta,\psi) = h(\theta,\psi) \quad \text{for } \theta \in [-90,-40]$$

$$H(\theta,\psi) = 0 \quad \text{for } \theta \in [-40,40]$$

$$H(\theta,\psi) = \frac{-h_{SH}}{h_{NH}} * h(\theta,\psi) \quad \text{for } \theta \in [40,90]$$

We consider values of A ranging from 0 to 35, every 5 W/m^2. $A = 0$ denotes the control cases, as no forcing is applied. In Fig. 1 we show the applied forcing pattern for the value of $A = 35$ W/m^2. The sign convention selected is positive out of sea. Therefore, positive values of the forcing could be thought as representing a situation where the atmosphere is dry and colder than the ocean below it.

To analyse the relative roles of the atmosphere, tropical SSTs and land surface temperatures in the response to the imposed forcing we perform 3 series of experiments. For each experiment setup there is a control run ($A = 0$) as well as perturbed runs (A different from zero). In the first series the slab ocean is applied globally. In the second series, the tropical (30°S–30°N) SSTs are kept fixed, while the slab ocean is applied elsewhere. In these first two experiments the slab land model is applied globally. Finally, in the third series the tropical (30°S–30°N) SSTs are kept fixed, the slab ocean model is applied elsewhere in the ocean and, also, the continental surface temperature over the African continent is kept fixed. In the experiments with fixed tropical SST, the prescribed tropical SSTs are the ones obtained in the control run with the global application of the slab ocean model. In the experiments with fixed surface temperature over Africa, the prescribed temperatures are the climatological temperatures of the land model. The experiments are named *global_slabs_A*, *fix_trop_SST_A* and *fix_trop_SST_fix_Africa_A*, respectively, with A denoting the strength of the forcing (varies from 0 to 35 W/m^2, every 5 W/m^2).

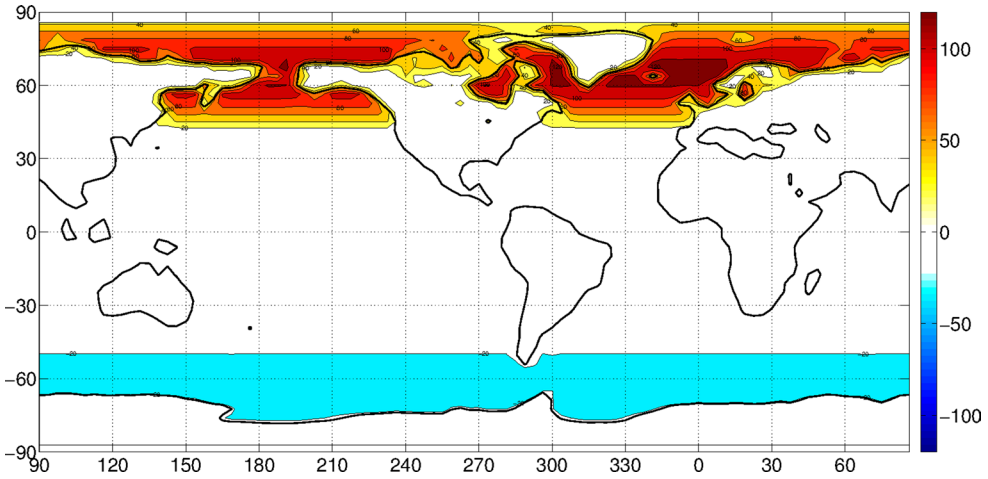

Fig. 1 Forcing pattern H, for $A = 35$ W/m^2. The sign convention is positive out of sea. *Contour interval* 20 W/m^2

Table 1 Experiment summary

Experiment name	Tropical SST fixed	Africa surface temperature fixed	Clear-sky longwave effect fixed
global_slabs_A	No	No	No
fix_trop_SST_A	Yes	No	No
fix_trop_SST_fix_Africa_A	Yes	Yes	No
fix_trop_SST_fix_cslw_A	Yes	No	Yes

A denotes the strength of the forcing (varies from 0 to 35 W/m^2, every 5 W/m^2)

Moreover, we perform a fourth experiment to elucidate the mechanisms responsibles for the African land surface temperature reaction to the extratropical forcing. This experiment is a variation of *fix_trop_SST_A* experiment in which, in addition to the tropical SSTs constraint we incorporate the restriction of fixed clear-sky longwave radiation (see Sect. 6). The experiment name is *fix_trop_SST_fix_cslw_A*. As with all the other experiments, a corresponding control case ($A = 0$) is calculated with this experiment configuration.

In all the simulations the model was run for 40 years and the last 10 are used for averaging. Running the simulations for 40 years proved to be more than enough to reach the equilibrium; a time scale of 10 years was estimated to be the time span necessary for adjustment (see Fig. 14). In Table 1 we summarize the four series of experiments.

3 Tropical sensitivity to extratropical forcing

In this section we present the results of the experiment where the slab ocean and land models are applied globally: *global_slabs_A*. First we analyse the precipitation response to variations in the parameter A. Second, we focus on the case with maximal strength of the forcing ($A = 35$ W/m^2) showing for different fields latitude–longitude, as well as zonal averages–height plots. These results are presented in the form of anomalies with respect to the associated control case (i.e. deviations of the forced run from the run with $A = 0$ and the same experiment configuration). Lastly, we show the meridional atmospheric energy transport.

In Fig. 2 we display the annual mean zonal averages of the precipitation anomalies for different values of the parameter A distinguishing total, oceanic and continental precipitation. Overall, the stronger the forcing the stronger the response in the zonal averages of the precipitation field. For total precipitation (Fig. 2a) the strongest responses are seen in the tropical region as well as in the northern high latitudes. In the tropics there are positive (negative) anomalies north (south) of 5°N, indicating a northward shift of the ITCZ. In this region, both the intensity as well as the meridional position of the maximum anomalies change with A: as A increases so does the magnitude of the anomalies and the meridional shift of the ITCZ is largest. It is worth noting that in this region the intensity of the response is not linear, showing a very weak signal for $A = 5$ W/m^2. In high latitudes of the NH the anomalies are positive and with increasing magnitude as A increases. For this region the changes in the parameter A influence the intensity of the response but not the meridional pattern of the zonally averaged anomalies. Decomposing the total precipitation into oceanic and continental components we see that the general behaviour is very similar: increasing A leads to an increase in the magnitude of the anomalies and, in the tropical region, also to a slight change in the meridional position of the maximum anomalies.

In the following we will focus on the results for the maximal strength of the forcing $A = 35$ W/m^2.

Near-surface air temperature (NSAT) anomalies are displayed in Fig. 3a. The response is a generalized warming in

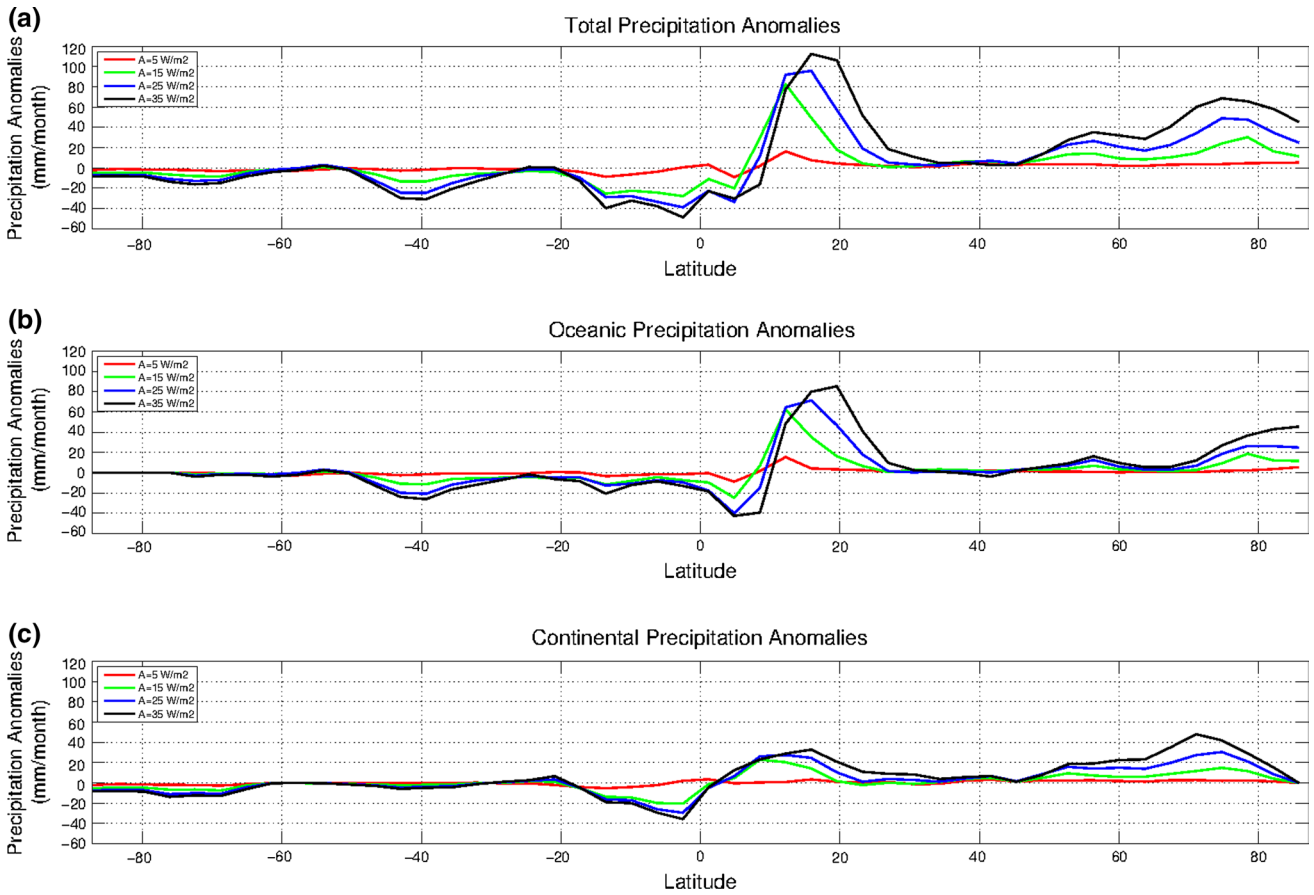

Fig. 2 Annual mean zonal averages of: **a** total precipitation anomalies. **b** Oceanic precipitation anomalies, **c** continental precipitation anomalies for several values of the parameter *A* and for the experiment with global slab ocean and land models: *global_slabs_A*

the NH and a generalized cooling in the SH, with the intensity of the warming/cooling largest towards high latitudes. Over sea maximum warming is about 17°C in the northern Atlantic while the maximum cooling can be found in the Southern Ocean with a value of −14 °C in the Amundsen Sea. The NSAT anomalies over sea in extratropics are quasi zonally symmetric. In the tropical region the main departures from the zonal symmetry can be found in the regions 20°N–30°N and 20°S–30°S in the Pacific Ocean where the zonal gradient is about 6 and 4 °C, respectively.

Over land the most extreme NSAT anomalies are seen over North America (up to 16 °C) and over Antarctica (around −8 °C). In latitudes lower than 30° the land response is most visible over the NH where the most extreme response is seen over the African continent (anomalies up to 10 °C centered at 25°N, 30°E), followed by the responses over North America (up to 5 °C anomalies) and Asia (up to 3 °C); in the SH low latitudes the signal is evident only over the Australian continent with negative anomalies of magnitude of the order of 1 °C.

Precipitation anomalies are shown in Fig. 3b. In the tropical Pacific and Atlantic oceans there is an increase (decrease) of precipitation north (south) of ~10°N, indicating a northward shift of the oceanic ITCZ, consistent with Fig. 2. The increase/decrease of precipitation is maximal toward the centre of the Pacific Ocean where it reaches ~350 mm/month. In the Indian Ocean there is no clear shift of the precipitation pattern. Continental precipitation is also affected, although in a weaker manner. A continental ITCZ displacement is also evident over both the African and the South American continents, with anomalies around 100 mm/month over Africa and 200 mm/month over South America. Extratropical precipitation changes are only important northward of 50°N (positive anomalies) and to the west of South America around 45°S (negative anomalies).

Near surface (950 hPa) wind anomalies are important only over ocean basins, in particular in the tropical Pacific and Atlantic Oceans, consistent with the ITCZ shift, and between 45°S and 60°S (Fig. 4a). In

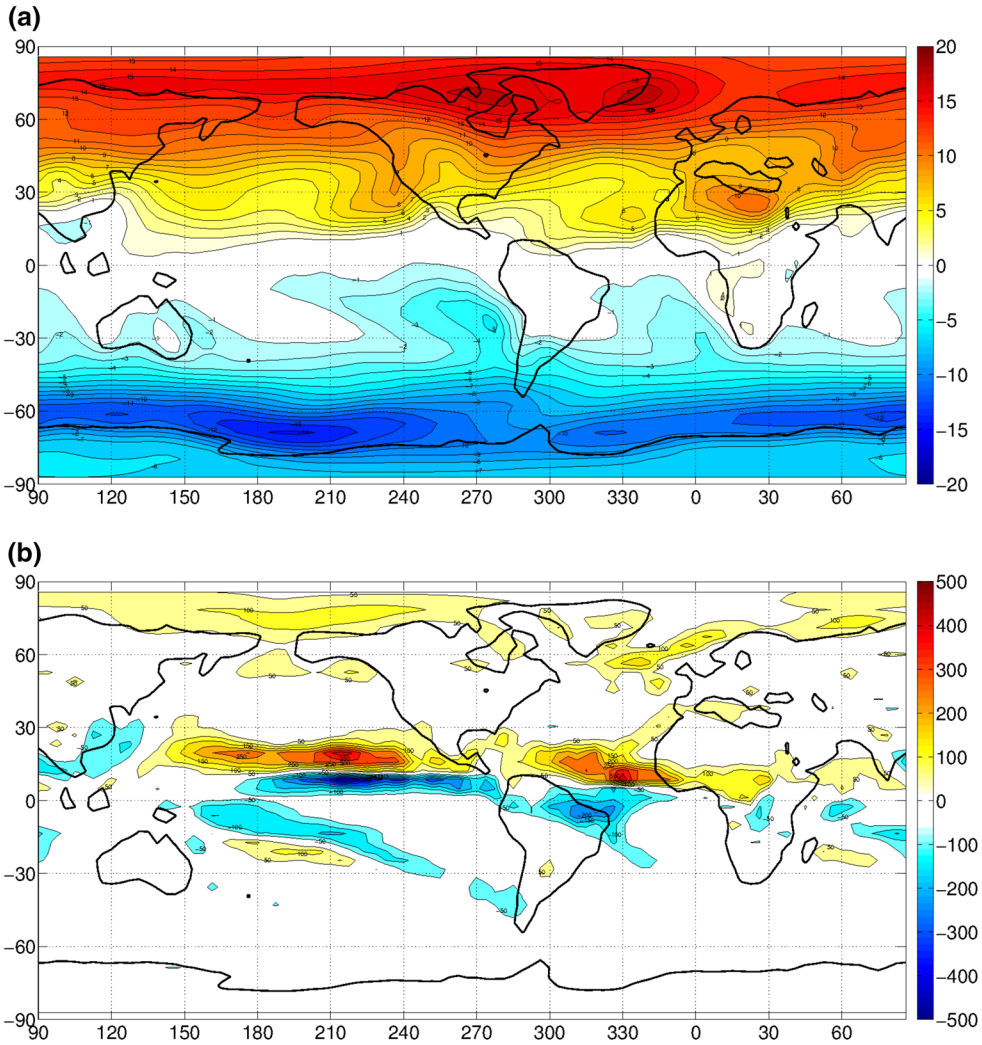

Fig. 3 Annual mean anomalies with respect to the control of: **a** NSAT (*contour interval* 1 °C), **b** precipitation (*contour interval* 50 mm/month) for the experiment with global slab ocean and land models and $A = 35$ W/m^2: *global_slabs_35*

the tropical Pacific the anomalies are located between 5°N and 20°N, exceeding the 10 m/s in the centre of the basin and with north-east direction. In the Atlantic the anomalies are located in the band 5°N–15°N being of importance (around 9 m/s) toward the west of the basin. Finally, in the Southern Ocean there is a band of westerly anomalies between 45°S and 60°S with intensities that range from 7 m/s to a maximum over 10 m/s in the region 190°E–240°E.

In upper levels the anomalous wind field shows easterly anomalies from 30°S until 60°N and westerly anomalies from 40°S until 60°S (Fig. 4b). The strongest anomalies are found in the region Equator-30°N and represent a weakening of the subtropical jet, consistent with a decrease in meridional temperature gradient. Thus, wind anomalies in the tropics are baroclinic and result from the change in the distribution of latent heat release due to the ITCZ shift. In the SH extratropics, on the other hand, the wind anomalies have a barotropic structure.

Next we show zonal averages, which will be denoted by square brackets. Temporal means will be denoted by an over bar and deviations from the temporal mean by primes.

Figure 5a displays anomalies with respect to the control run of the zonally averaged zonal wind ($[\bar{u}]$). There are two distinct anomaly patterns. The first one is a region of positive anomalies located in the latitude band 60°S–40°S with a clear barotropic structure and a maximum of 12 m/s located near the 200 hPa level between 60°S and 50°S. The second one is a region of negative anomalies that comprises the latitudes 10°S–80°N upward from the 500 hPa level, with a maximum of 15 m/s at 20°N and 200 hPa.

To get insight into the mean meridional circulation it is useful to consider the mass streamfunction Ψ_M defined as

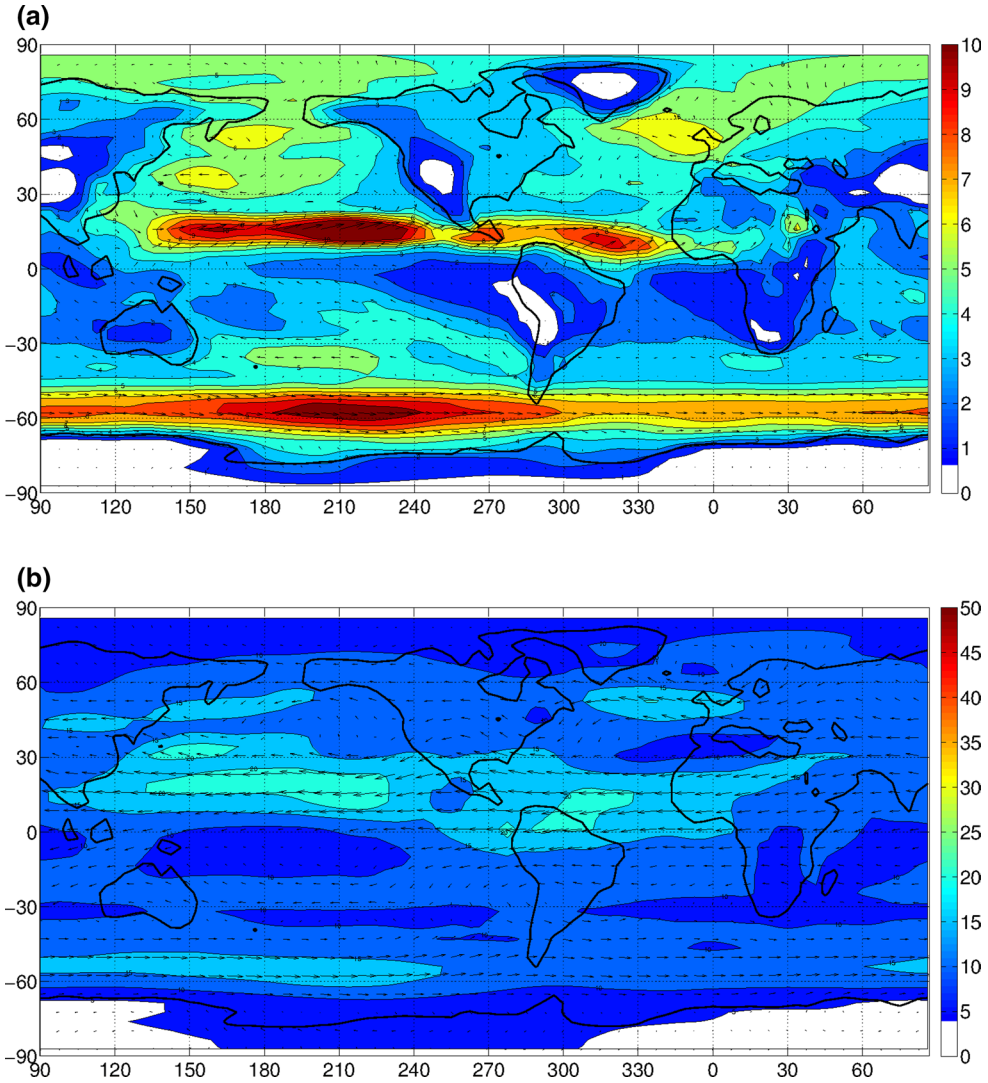

Fig. 4 Annual mean anomalies with respect to the control of: **a** wind at 950 hPa (*arrows* indicate wind direction, *colors* indicate wind magnitude, *contour interval* 1 m/s), **b** wind at 200 hPa (*arrows* indicate wind direction, *colors* indicate wind magnitude, *contour interval* 5 m/s) for the experiment with global slab ocean and land models and $A = 35$ W/m^2: *global_slabs_35*

(e.g. Hartmann 1994): $\Psi_M = \frac{2\pi a \cos(\theta)}{g} \int_0^p [v] dp$ where a is Earth's radius, θ the latitude, g gravity, p pressure and v meridional wind. In Fig. 5b we present the changes with respect to control of the mean meridional overturning circulation stream function $[\Psi_M]$. Negative anomalies in the tropical region indicate a northward displacement of the uplift region along with an intensification of the southern Hadley cell and a weakening of the northern Hadley cell. Although much weaker there is also a response in the Ferrel cells: the southern cell is intensified and the northern cell weakened.

Anomalies of meridional momentum transport performed by eddies $\left([\overline{u'v'}]\right)$ are only of importance above 700 hPa and mostly negative, with one maximum in each hemisphere (Fig. 5c). In the SH the anomalies are maximum between 60°S and 40°S with magnitudes that exceed the 30 m^2/s^2, while in the NH the maximum anomalies are weaker and located closer to the Equator (between 40°N and 30°N) with a maximum of 10 m^2/s^2. These negative anomalies imply an intensification (weakening) of the transport from the tropics to high latitudes in the SH (NH). In addition, it is worth noting that such fluxes drive a poleward intensification of the zonal flow in the SH: as (e.g. Holton 2004) $\frac{du}{dt}\alpha - \frac{d[\overline{u'v'}]}{dy}$ in the case shown by Fig. 5c, the meridional gradient of $[\overline{u'v'}]$ is positive (negative) on the equatorward (poleward) side of the minimum centered at (50°S, 250 hPa), forcing a poleward shift of the mid-latitude jet in the SH. The latitude of strengthening of the mid-latitude jet coincides with the latitude of maximum SST gradient anomaly (50°S–60°S) consistent with the driving role of the lower atmosphere temperature gradient in the behaviour of the jet (e.g. Lorenz and Hartmann 2001).

In Fig. 5d we show the anomalies of the meridional heat transport by eddies $\left([\overline{v'T'}]\right)$. The anomalies are fundamentally negative, maximal in the latitude bands 60°S–40°S and 40°N–60°N close to surface and also at the jet level. The SH anomaly is stronger than the northern counterpart. As was

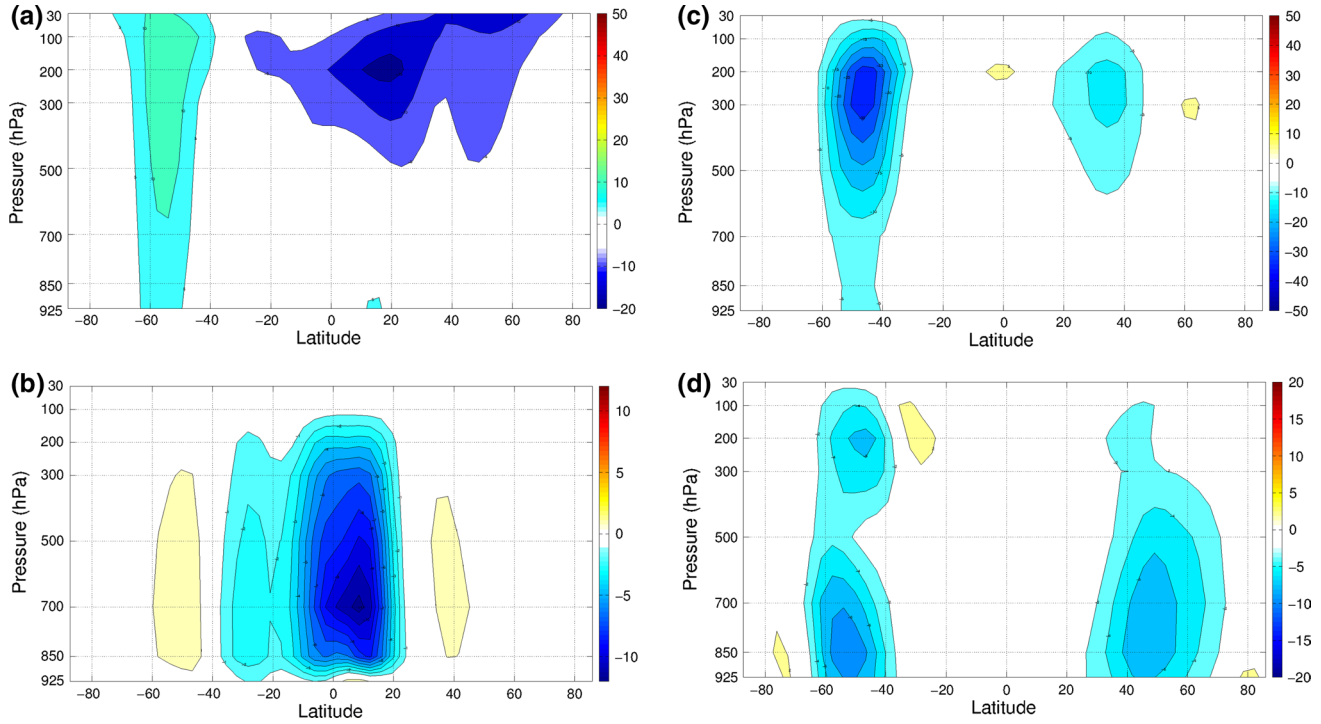

Fig. 5 Annual mean anomalies with respect to the control of: **a** zonally averaged zonal wind with height $[\bar{u}]$ (*contour interval* 5 m/s), **b** mean meridional overturning circulation stream function $[\overline{\Psi_M}]$ /10^{10} (*contour interval* 1 kg/s), **c** mean meridional momentum transport by eddies $[\overline{u'v'}]$ (*contour interval* 5 m^2/s^2), **d** mean meridional heat transport by eddies $[\overline{v'T'}]$ (*contour interval* 2 mK/s) for the experiment with global slab ocean and land models and $A = 35$ W/m^2, *global_slabs_A*

the case with momentum transport, these negative anomalies imply an intensification (weakening) of the eddy heat transport form the tropics to high latitudes in the SH (NH).

Finally, Fig. 6a displays the meridional atmospheric energy transport for the control case and the experiment with $A = 35$ W/m^2. As previous studies have shown (e.g. Schneider et al. 2014) the energy flux equator is displaced northward in the forced case, as the atmospheric transport diminishes (increases) towards the NH (SH).

4 Role of the tropical SST

In this section we present the results of the experiment where the tropical SST are kept fixed and the slab ocean model is applied elsewhere, the land model is applied globally: *fix_trop_SST_A*. The anomalies are calculated with respect to the associated control case. Again, we start by analysing the dependence of zonal precipitation anomalies on the intensity of the forcing. We then focus the analysis on the case with the maximum forcing, $A = 35$ W/m^2.

Figure 7 shows the annual mean zonal averages of the precipitation anomalies (distinguishing total, oceanic and continental precipitation) for the experiment *fix_trop_SST_A* for different values of A. For the total precipitation field the most important anomalies occur in high latitudes of the NH. In this region, the stronger the forcing the stronger the positive precipitation anomalies and no meridional changes in the anomalous response are evident with the increase of A. The mechanism behind this behaviour is possibly related to the increase in specific humidity due to the warming of the region (not shown). Meanwhile, in the tropics the response is much weaker than that obtained for the experiments with global slab ocean and land models, although the signal is not null. We should note that close to the Equator there is a weak positive (negative) anomaly north (south) of 5°N, that could indicate a timid response of the ITCZ, slightly shifting to the north. The decomposition of total precipitation into oceanic and continental indicates that both components present the stronger response in the NH high latitudes (both with positive anomalies increasing in magnitude with A); in the tropical sector the oceanic precipitation displays weak negative anomalies from the Equator to 10°N while in the continental part some positive and also weak anomalies are seen from 10°N to 20°N.

As increasing the intensity of the forcing pattern mainly led to an increase in the response we will now only analyse more in detail the response for the maximal strength of the forcing $A = 35$ W/m^2.

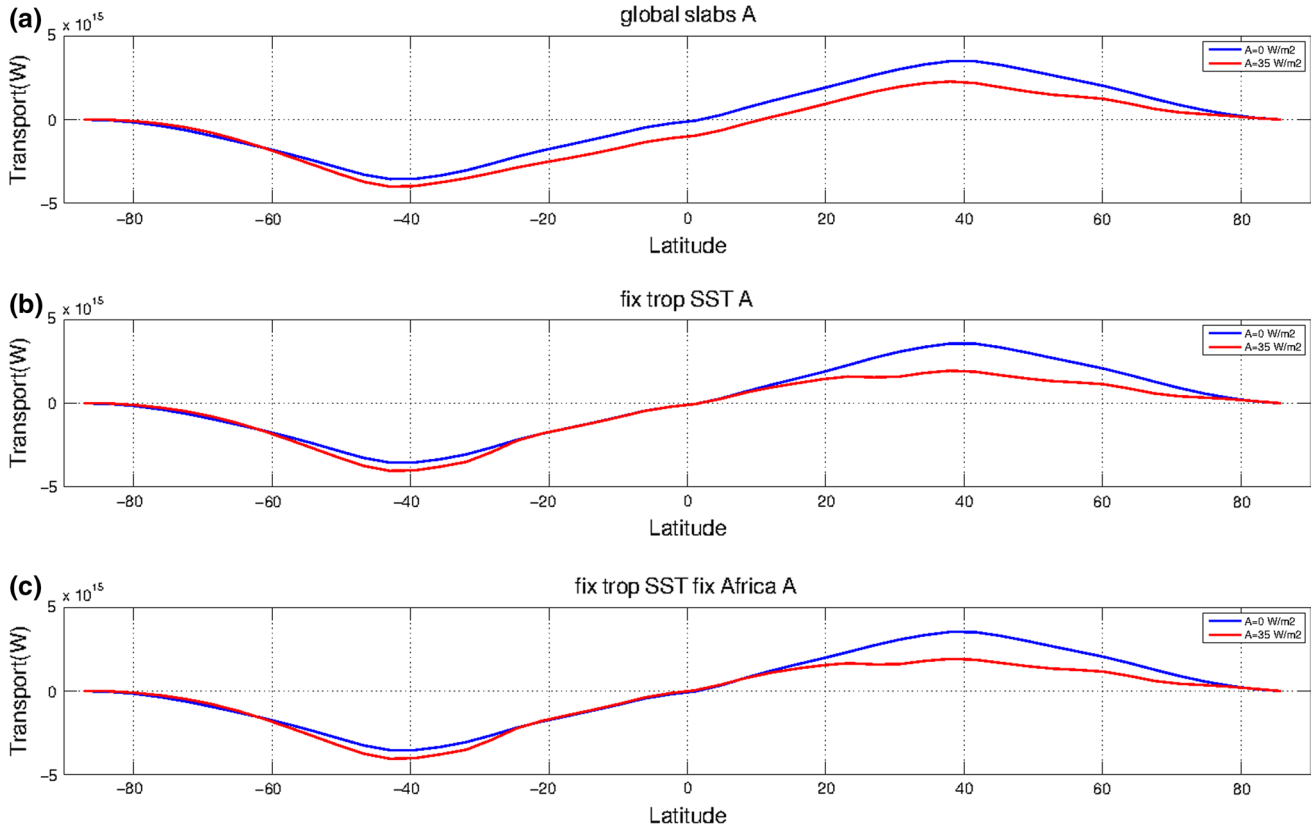

Fig. 6 Northward atmospheric energy transport for the experiments: **a** *global_slabs_A*, **b** *fix_trop_SST_A* and **c** *fix_trop_SST_fix_Africa_A* for $A = 0$ (control cases) and $A = 35$ W/m^2

NSAT anomalies are depicted in Fig. 8a. Evidently, anomalies over sea in the tropics are zero given that the prescribed SST for that region coincides with the SST of the corresponding control case. Over the oceans the anomalies are positive (negative) in the northern (southern) extratropics, with increasing absolute magnitude toward the poles. For both hemispheres the anomalies over sea are very close to being zonally symmetric although there are some asymmetries in the Southern Ocean and to the west of the North American continent.

As was the case with the experiment *global_slabs_A* there is a generalized continental warming (cooling) in the NH (SH). In extratropics the response is very similar to the one obtained in the previous experiment (compare Figs. 3a and 8a). However, some differences are seen in particular with the extent of the continental warming in the region equatorward of 30°N: in Asia now the warming only reaches 1 °C, in North America 3 °C and in Africa 8 °C, hence, indicating a 2 °C lower response than in the experiment with the global slab ocean model.

Precipitation anomalies in extratropics are very similar to the ones obtained when the tropical SST restriction was not imposed (Fig. 8b). On the other hand, the tropical response is very different: the only place where there are signs of a northern shift in the ITCZ is over equatorial western Africa and over the Atlantic Ocean, with anomalies of the order of 50 mm/month. To better quantify the changes in precipitation we select three tropical precipitation indices: precipitation anomalies over the Sahel (8°N–15°N, 350°E–30°E), precipitation anomalies over the tropical Atlantic Ocean (5°N–12°N, 322°E–341°E; considering northern half minus southern half) and precipitation anomalies over South America (10°S-Eq. 300°E–322°E). Figure 9 indicates the regions considered. In Table 2 we calculate the values of those indices for the experiment *fix_trop_SST_35* relative to the same indices for the experiment *global_slabs_35*. We see that over Africa the response in the experiments with fixed tropical SST represents more than half (58 %) of the response obtained when the slab ocean model is applied globally, indicating that for this region the tropical SSTs are important but not crucial in determining changes of precipitation forced by an extratropical source. On the other hand, over the Atlantic Ocean and South America the response in the experiments with restricted tropical SST has a magnitude of 19 and 13 %, respectively, of the response obtained without such restriction, therefore indicating that for these regions the role of the tropical SSTs is much more important.

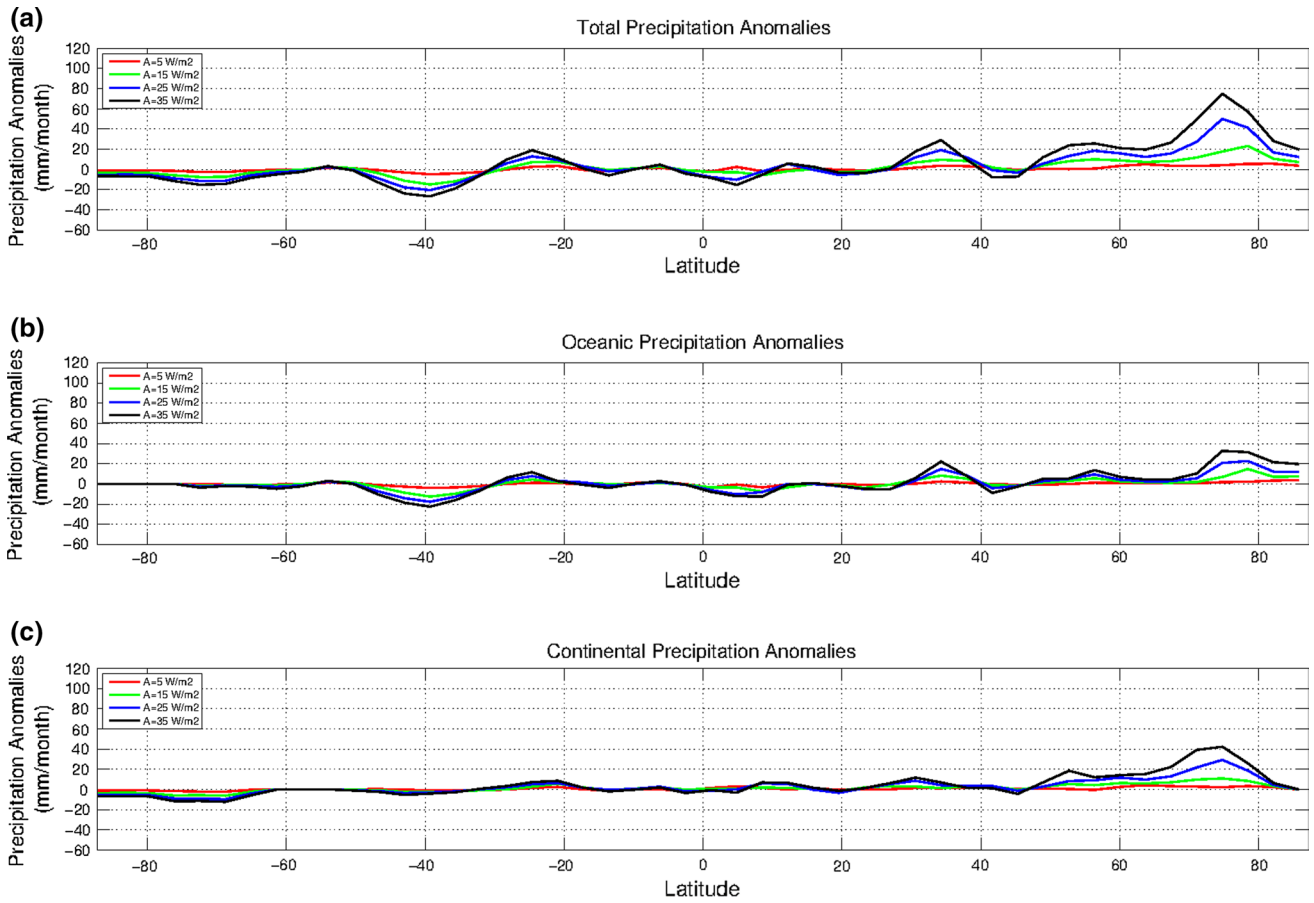

Fig. 7 Same as Fig. 2 for the experiment with fixed tropical SST, global slab land: *fix_trop_SST_A*

As expected, tropical surface and upper level wind anomalies in this experiment are practically null (Fig. 10a, b), with the exception of some southwesterly surface anomalies over east Africa in the latitude band Equator-15°N. The extratropical anomalies are very similar in structure to those obtained when the slab ocean model is applied globally, although in upper levels in the NH a slight weakening of the mid-latitude jet can be appreciated.

Figure 11a shows the zonally averaged zonal wind ($[\bar{u}]$) anomalies with respect to the corresponding control run. Once again, the main difference with the experiment applying the slab ocean model globally is that the tropical anomalies almost vanish. In extratropics, the SH barotropic and positive anomaly pattern is still present showing an increase in the mid latitude jet; in the NH extratropics the negative anomaly is slightly stronger and evidences the weakening of the jet.

Regarding the mean meridional circulation changes, seen through $[\overline{\Psi_M}]$ anomalies, it is evident that the Hadley circulation is almost not affected with the tropical SST constraint imposed in this experiment (Fig. 11b).

The eddy meridional momentum and heat fluxes are displayed in Fig. 11c, d, respectively. In both transports there is a subtle weakening of the transport from the tropics to the Poles, with respect to the experiment with global slab ocean model application.

The meridional atmospheric energy transport for this experiment is shown in Fig. 6b. On the contrary of what occurred in the experiments *global_slabs_A*, the energy flux equator does not show any appreciable displacement from the control case when the forcing is applied, consistent with the fact that the ITCZ shifts are negligible when averaged zonally.

Bearing in mind the precipitation anomalies shown in Fig. 8c, which shows that the main tropical response to the extratropical forcing when the tropical SSTs are kept fixed and $A = 35$ W/m^2 is a northern shift in the ITCZ over western Africa and the Atlantic Ocean, in Fig. 12

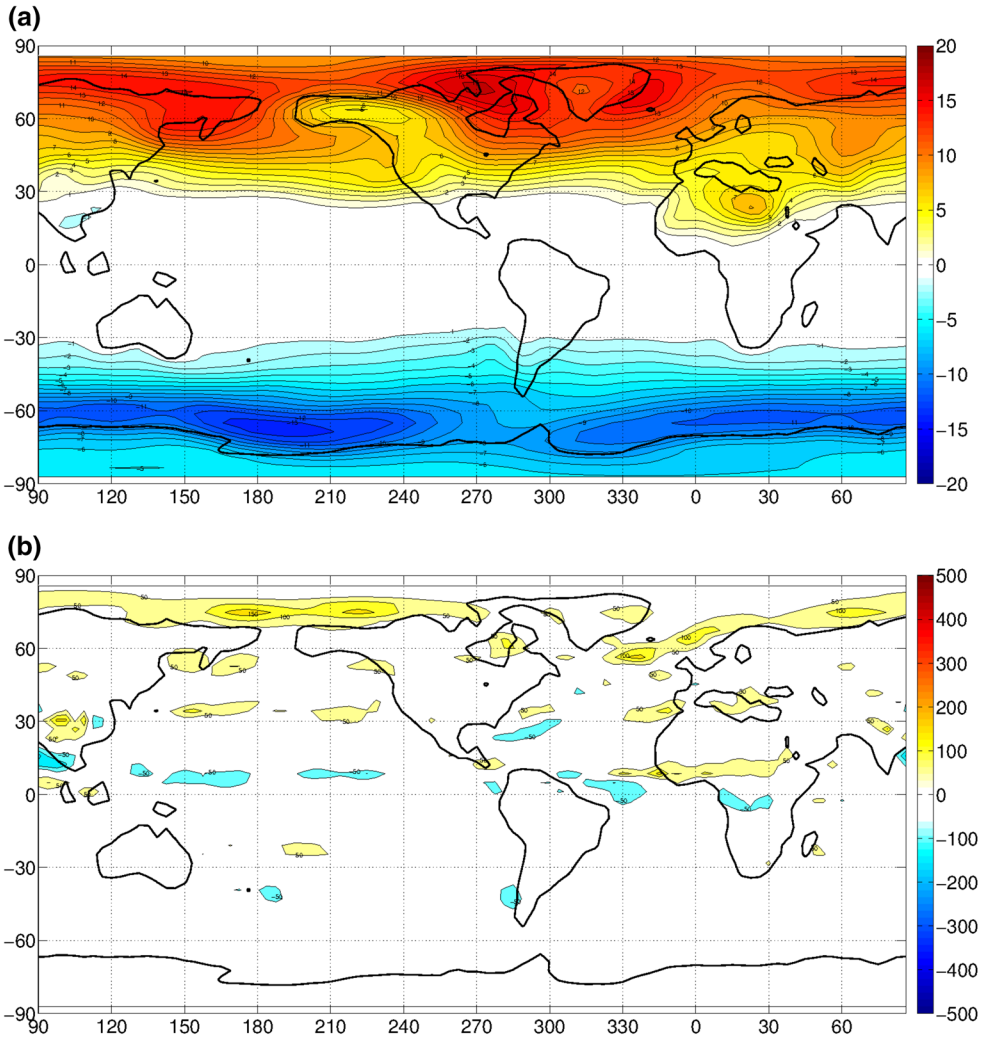

Fig. 8 Same as Fig. 3 for the experiment with fixed tropical SST, global slab land: *fix_trop_SST_35* except that the control run is the one corresponding to this experiment setup

we restrict the view to that tropical sector (300°E–30°E) and show the total, oceanic and continental zonal mean precipitation variations with the parameter A in that region. For this restricted tropical sector we clearly see that the ITCZ response seen for the case of maximal strength of the forcing is still present for lower values of A. The ITCZ response consists in a northward displacement, increasing in magnitude with the strength of the forcing and is mostly due to the continental precipitation signal.

In summary, from the results of this sub section, we can conclude that when the extratropical forcing is applied and the tropical SST is not allowed to react in consequence, the tropical precipitation response is weak but still not negligible, specially over Africa and the Atlantic Ocean where the ITCZ shows a northward displacement which increases its magnitude with the strength of the forcing. This tropical response is more important over the continent than over the ocean and seems related to the fact that the surface temperature over the African continent is greatly affected by the forcing while the SSTs are maintained fixed. With this motivation, in the next section we show the results for a series of experiments where, in addition, the surface temperature over Africa is kept fixed.

5 Role of African continental temperature

In this section we present the results of the experiment where the tropical SST are kept fixed (the slab ocean model is applied elsewhere) and the surface land temperature over Africa is kept fixed, applying the slab land model elsewhere: *fix_trop_SST_fix_Africa_A*. As was the case before, anomalies are calculated with respect to the corresponding control case and we will only show the results for the maximum strength of the forcing $A = 35$ W/m^2. For this experiment we will focus on the fields: NSAT, precipitation and atmospheric meridional energy transport as the other fields investigated

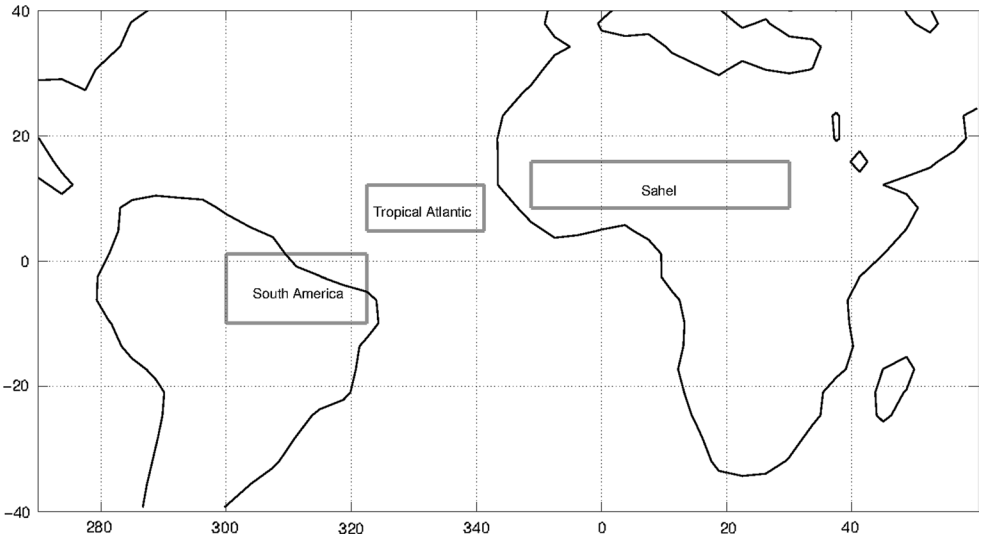

Fig. 9 Regions where the precipitation indices are calculated: Sahel (8°N–15°N, 350°E–30°E), Tropical Atlantic (5°N–12°N, 322°E–341°E) and South America (10°S-Eq. 300°E–322°E)

Table 2 Value of the Sahel, Tropical Atlantic (northern half minus southern half) and South America precipitation indices for the experiments *fix_trop_SST_35* and *fix_trop_SST_fix_Africa_35* relative to the values for the experiment *global_slabs_35*

	Sahel (%)	Tropical Atlantic (%)	South America (%)
fix_trop_SST_35	58	19	13
fix_trop_SST_fix_Africa_35	15	4	11

previously show little change with respect to the experiment where the tropical SSTs were fixed.

The NSAT anomalies over sea do not differ between the experiments *fix_trop_SST_fix_Africa_35* and *fix_trop_SST_35* (Fig. 13a vs. Fig. 8a). Differences in tropical temperatures are however seen over land as temperatures over Africa are prescribed (Fig. 13a vs. Fig. 8a).

In Fig. 13b, we show the precipitation anomalies. For this experiment tropical precipitation changes are almost not present, in particular the anomalies over Africa and the tropical Atlantic are essentially zero. On the contrary, in the extratropics, the anomalies are very similar to those obtained without constraining the African land temperatures. For a more quantitative vision in Table 2 we calculate the values of the precipitation indices (Sahel, Atlantic and South America) for the experiment *fix_trop_SST_fix_Africa_35* relative to the same indices for the experiment *global_slabs_35*. For this experiment we see that the precipitation responses are very weak compared with the experiment in which the two slab models are applied globally and never exceed 15 % in magnitude, indicating that when both the tropical SSTs and the surface land temperatures are not allowed to react to the extratropical forcing, the precipitation response almost vanishes. Moreover, comparison among the indices clearly indicates that rainfall over the Sahel is the one that is most influenced by the surface warming over Africa. The Atlantic ITCZ shift is also controlled by the African temperatures, while precipitation over South America shows almost no response.

6 Physical mechanisms: teleconnection between extratropics and African land surface temperature

As we have shown in the previous section, the role of the land surface temperature over Africa is essential for obtaining an ITCZ response to the imposed extratropical forcing when the tropical SSTs are not allowed to react. Hence, in this section we try to answer the question: what are the physical mechanisms that make the African land surface temperature change once the extratropical forcing is imposed?

We start by analysing the surface energy balance in the experiment *fix_trop_SST_35* in the region of the maximum African land surface temperature response (15°N–30°N, 15°E–30°E).

Surface fluxes play a key role in the land temperature response. Thus, to validate model results we first determine how well the control run (*fix_trop_SST_0*) simulates the surface energy fluxes in this African region. Table 3 presents a comparison with two reanalysis products: NCEP-NCAR (Kalnay et al. 2006) and ERA40 (Uppala et al.

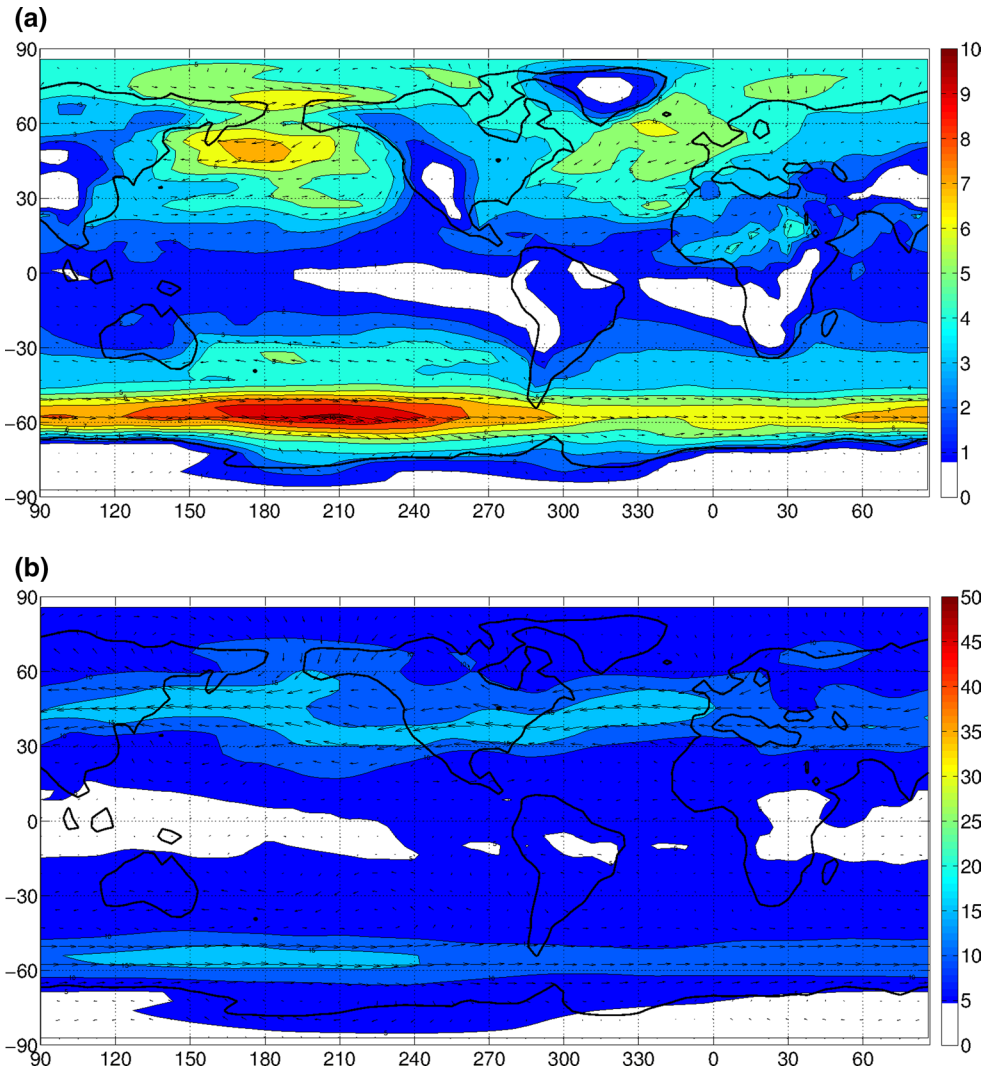

Fig. 10 Same as Fig. 4 for the experiment with fixed tropical SST, global slab land: *fix_trop_SST_35* except that the control run is the one corresponding to this experiment setup

2005), using data from years 1979 to 2001. The values for net shortwave radiation are quite different in the reanalysis and the model value lies between them. On the other hand, the net longwave radiation has similar magnitudes in both reanalysis products as well as in the simulation. The sensible heat term is the one with largest difference between reanalysis products (a factor of 2), and the simulation result for this term lies between the values given by the two reanalysis. Lastly, the latent heat flux term is practically negligible in the reanalysis and in the simulation, although the simulation somewhat overestimates the value given by the reanalysis. Thus, overall, the model simulates the surface energy balance adequately.

Figure 14 displays, for the region of maximum temperature response, the annual-means of average land surface temperature anomalies and the terms of the surface energy balance: net shortwave radiation, net longwave radiation, sensible heat flux and latent heat flux. As can be seen in the land surface temperature time series, the stationary state is reached after ~10 years of simulation with an average warming of 5–6 °C. The same time scale for equilibrium is seen in all the terms of the surface energy balance. However, the net surface heat flux is nonzero even after the stationary state has been reached. This is because the energy equation in the land model posses a small damping term with a time scale of 40 days to prevent the land surface temperature to drift away from the climatological mean (Molteni 2003). This damping term is small compared to the other terms involved in the energy balance, with exception of the latent heat flux, which does not play a role here. For example, for the region of interest (15°N–30°N, 15°E–30°E) in the experiment *fix_trop_SST_0* (*fix_trop_SST_35*) the corrective term is of the order of 7 W/m^2 (11 W/m^2). Hence, except for the damping term, Fig. 14 shows that the energy balance is reached mainly between the radiative terms, with the sensible heat flux playing a secondary role. The sum of the radiative terms plus the sensible heat flux is directed downward, in the same direction

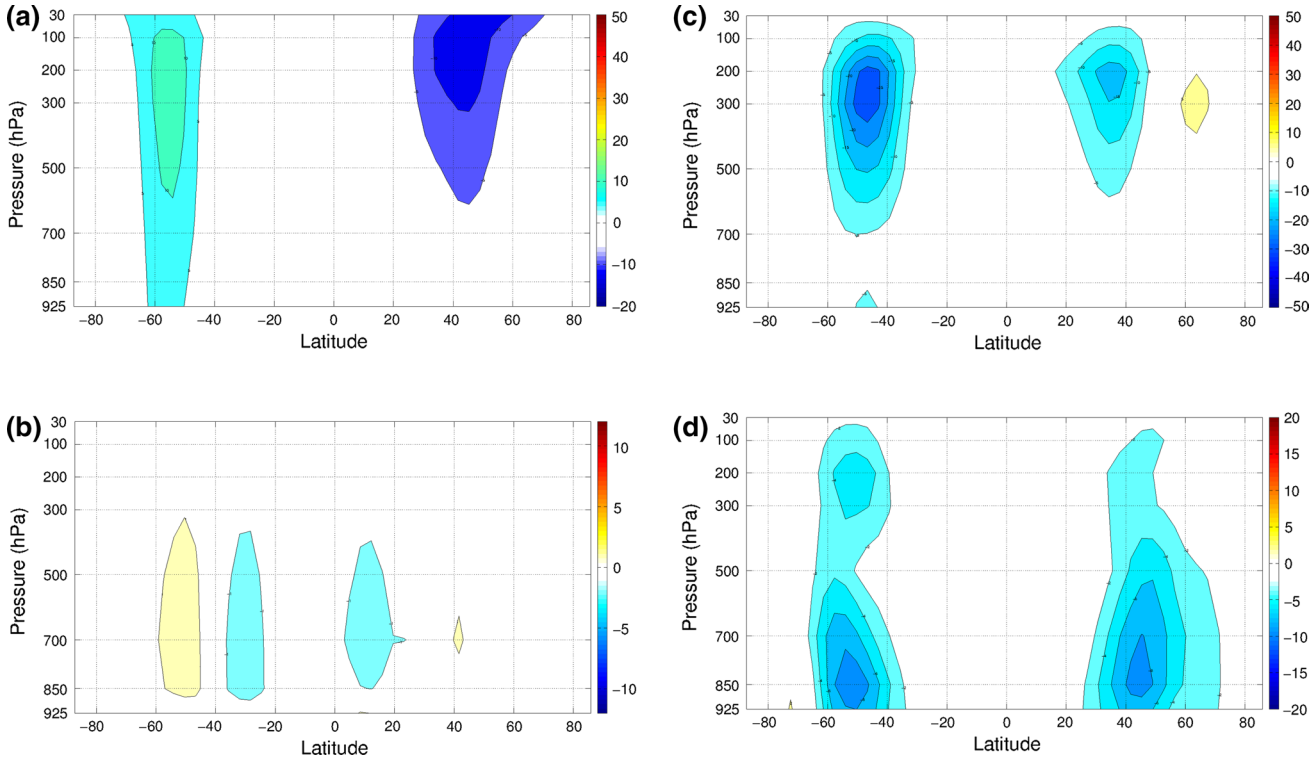

Fig. 11 Same as Fig. 5 for the experiment with fixed tropical SST, global slab land: *fix_trop_SST_35* except that the control run is the one corresponding to this experiment setup

as the longwave radiation. Thus, the warming of the continent in this region appears to be related to the longwave radiation effect.

The longwave radiation effect can be decomposed into clear-sky and cloud components. Given that cloud changes are not particularly important in the region, we speculate that the clear-sky component must be the one playing the dominant role. To demonstrate this we designed a new experiment (*fix_trop_SST_fix_cslw_A*) in which, in addition to the prescribed tropical SSTs, the clear-sky component of the longwave radiation is maintained fixed globally. Again, we perform runs in which the extratropical forcing is applied (A different from zero), as well as an associated control run ($A = 0$, i.e. no forcing), all of them sharing the same experimental configuration.

In the parametrization scheme for longwave radiation [see Molteni (2003) for more details] the infrared spectrum is partitioned into four bands: between 8.5 and 11 μm, the band of strong absorption by CO_2, the aggregation of regions with weak or moderate absorption by water vapour and the aggregation of regions with strong absorption by water vapour. For each band and model layer a transmissivity is computed as a function of layer depth, specific humidity and cloud properties. The effect of clouds is modeled as a decrease in the transmissimity in the first band. To inhibit clear-sky longwave changes, we modify the transmissivity in the two water vapour bands, replacing in the transmissivity computation at each time step the calculated specific humidity by a climatological specific humidity (in this case climatology is obtained computing the monthly averages of the last 10 years of simulation of the control run).

As Fig. 14, Fig. 15 displays the results for the experiment with fixed clear-sky longwave radiation: *fix_trop_SST_fix_cslw_35*. The time-scale to achieve the stationary state is unchanged (~10 years). The land surface temperature response is still of warming but more moderate (values between 3 and 4 °C) while the predominant terms in the surface energy balance are the shortwave radiation and the sensible heat flux.

Finally, in Fig. 16 we show the NSAT and precipitation anomalies (with respect to the associated control case) for the experiment with prescribed tropical SSTs and clear-sky longwave radiation. Over sea, the NSAT response is very similar to the one obtained without the restriction over the longwave radiation. On the other hand, the NSAT anomalies over Africa

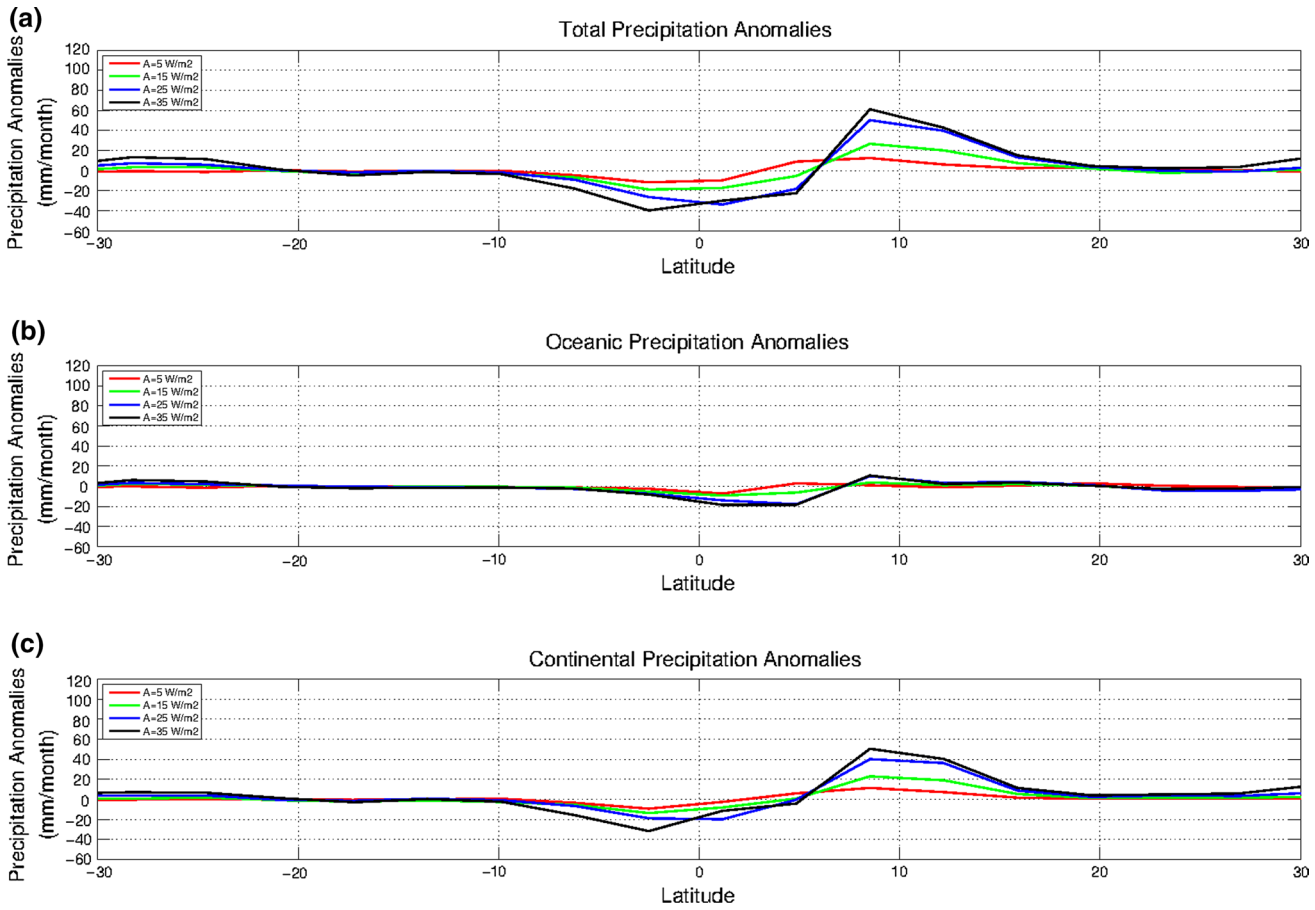

Fig. 12 Annual mean zonal averages in the region 300°E–30°E of: **a** total precipitation anomalies, **b** oceanic precipitation anomalies, **c** continental precipitation anomalies, shown in the tropical sector (30°S–30°N) for several values of the parameter *A* and for the experiment with fixed tropical SST, global slab land: *fix_trop_SST_A*

are clearly weaker, with a maximum of 5 °C over central Sahara desert, while the ITCZ response is almost completely suppressed (Fig. 8 vs. Fig. 16).

So, how does the African land surface temperature change once the extra-tropical forcing is imposed? We hypothesize the following mechanism. Once the forcing is imposed, a general warming occurs in the region of application in the NH (poleward of 40°N), leading to an increase in the specific humidity there (not shown). Changes in the circulation advect humidity towards the African continent (note the westerly anomalies from the Atlantic into the Sahara in Fig. 10), therefore increasing the humidity there and enhancing the clear-sky longwave greenhouse effect that leads to a warming of the surface beneath. As the warming is associated with a decrease in the regional sea level pressure (not shown) it drives the ITCZ northward over the continent. Some other processes may also play a role in explaining the remaining warming.

7 Summary and conclusions

We investigated the response of the ITCZ to extratropical forcing in an AGCM coupled to slab ocean and land models, with realistic surface boundary conditions. We imposed an oceanic heat flux forcing, with zero global mean, consistent of warming in the NH and cooling in the SH and analysed the changes obtained when averaging over a 10-year period. The relative roles of the atmosphere, tropical SSTs and continental surface temperature over Africa were investigated in three series of experiments. Finally, the mechanisms behind the land-based extratropical to tropical communication were studied.

In the simulation where the slab ocean and land models are applied globally our results are consistent with previous results in the sense that the ITCZ shifts toward the warmer hemisphere and that the magnitude of the shift increases with the magnitude of the forcing. In this case we

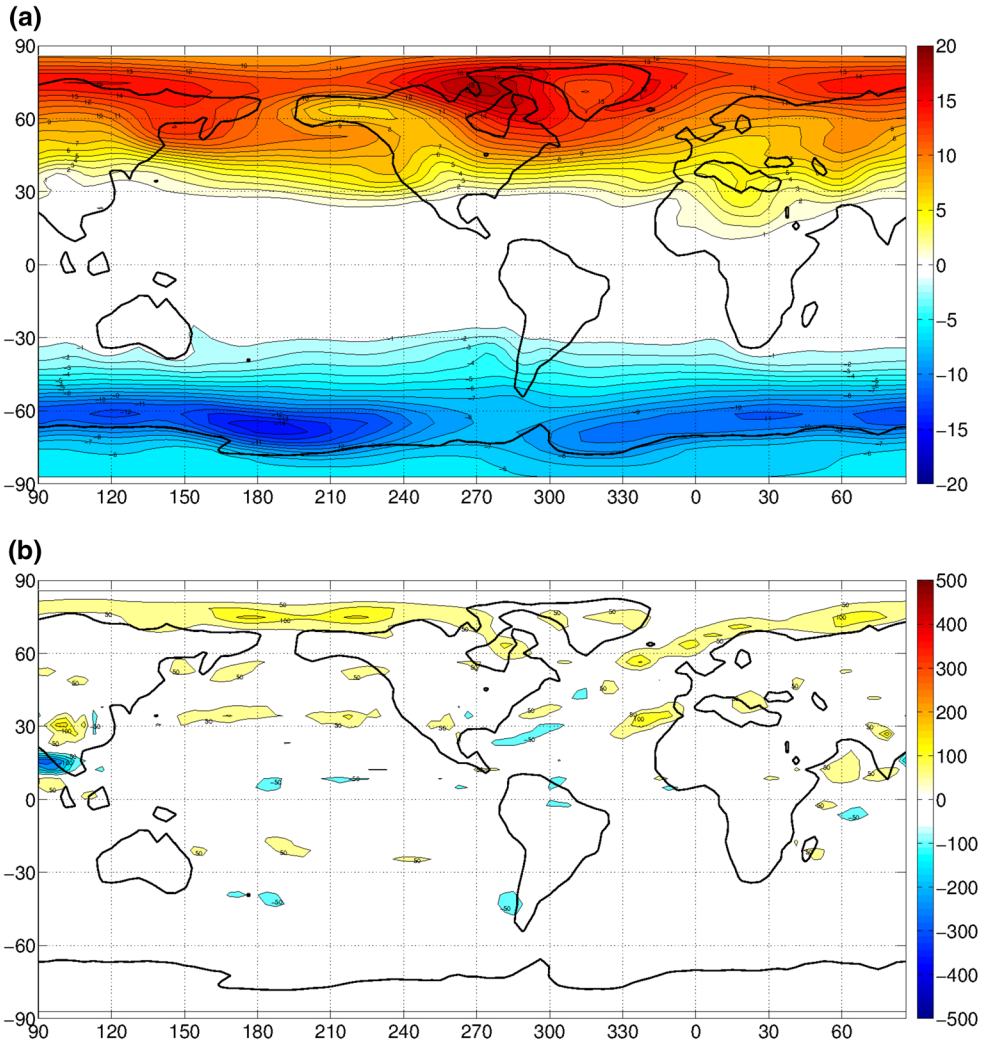

Fig. 13 Same as Fig. 3 for the experiment with fixed tropical SST, fixed surface temperature over Africa: *fix_trop_SST_fix_Africa_35* except that the control run is the one corresponding to this experiment setup

also attribute the ITCZ displacement mainly to the tropical cross-equatorial SST gradient, a finding consistent with previous studies. However, some aspects of our simulations differ from previous works: in particular, we found that the magnitude of the tropical precipitation zonal mean maximum increases with the magnitude of the forcing at the same time that no changes to the width of the ITCZ are noticed, while Kang et al. (2008) found that this maximum gets weaker and the ITCZ widens. As has been shown before the ITCZ control by the SST results extremely sensitive to the deep-convection scheme implemented (e.g. Liu et al. 2010; Song and Zhang 2009; Lin 2007) and, as a consequence, we hypothesize that the differences found might be due the use of different AGCMs, and therefore different parameterizations. Switching between realistic surface boundary conditions and an aqua-planet configuration might also play a role. With respect to heat and momentum atmospheric transports we found that both react to the extratropical forcing by increasing (decreasing) the amount transfered from the tropics to the SH (NH) in order to compensate the anomalous cooling (warming) of the

Table 3 Annual mean values of surface net shortwave radiation, net longwave radiation, sensible heat flux and latent heat flux in the region (15°N–30°N, 15°E–30°E) for NCEP-NCAR reanalysis (years 1979–2001), ERA40 Reanalysis (years 1979–2001) and the experiment *fix_trop_SST_0*

	NCEP-NCAR reanalysis	ERA40 reanalysis	*fix_trop_SST_0*
Net shortwave radiation (W/m^2)	210	149	200
Net longwave radiation (W/m^2)	115	111	127
Sensible heat flux (W/m^2)	86	38	52
Latent heat flux (W/m^2)	8	3	14

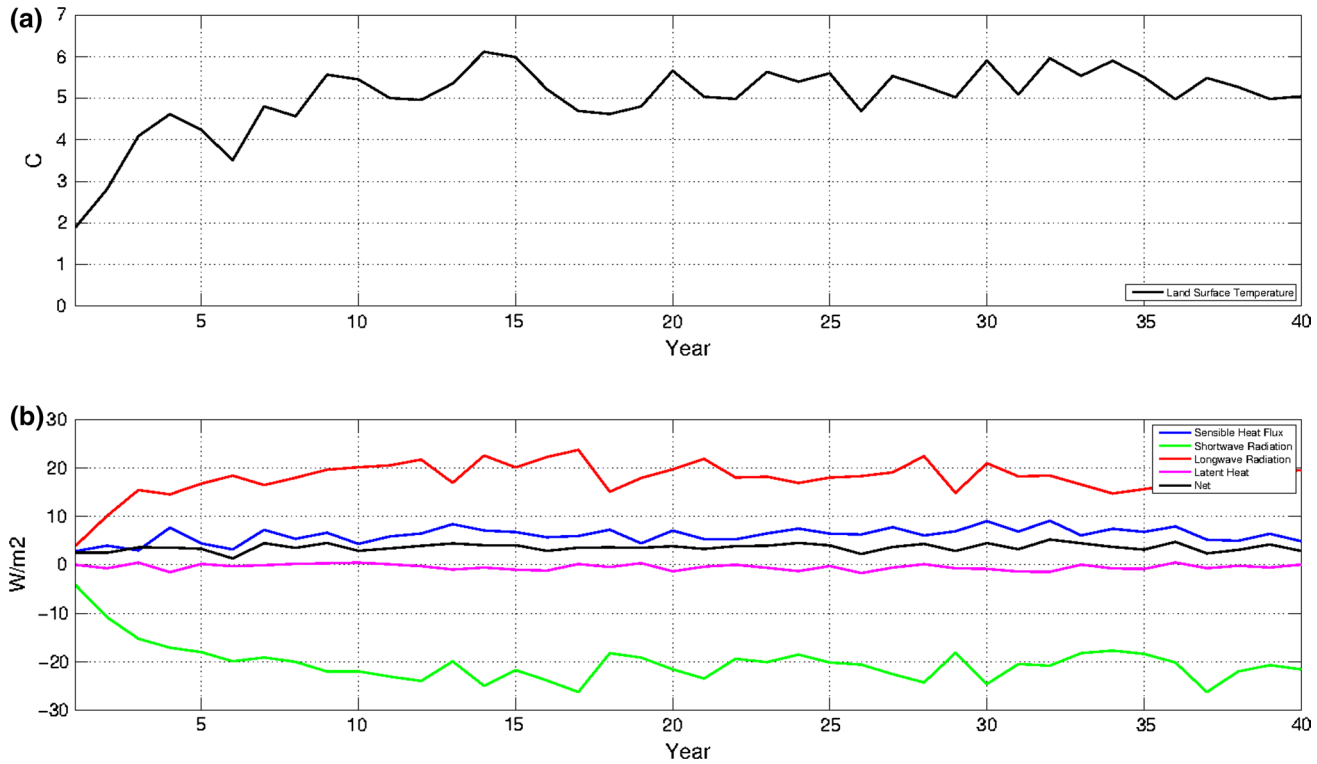

Fig. 14 Annual mean anomalies with respect to the control of: **a** land surface temperature, **b** shortwave radiation, longwave radiation and sensible heat flux, in the region (15°N–30°N, 15°E–30°E) for the experiment *fix_trop_SST_35*

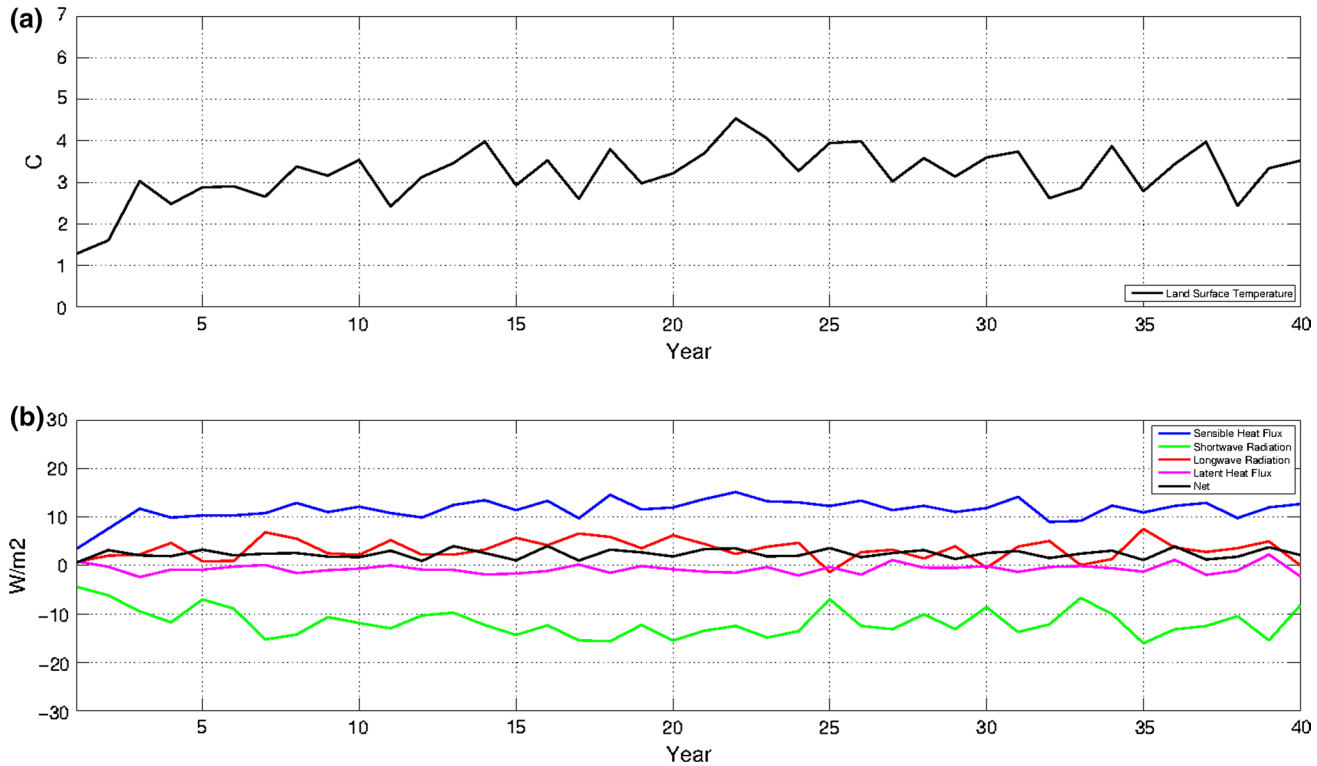

Fig. 15 Same as Fig. 14 for the experiment with fixed tropical SST, global slab land and fixed clear-sky longwave radiation *fix_trop_SST_fix_cslw_35* except that the control run is the one corresponding to this experiment setup

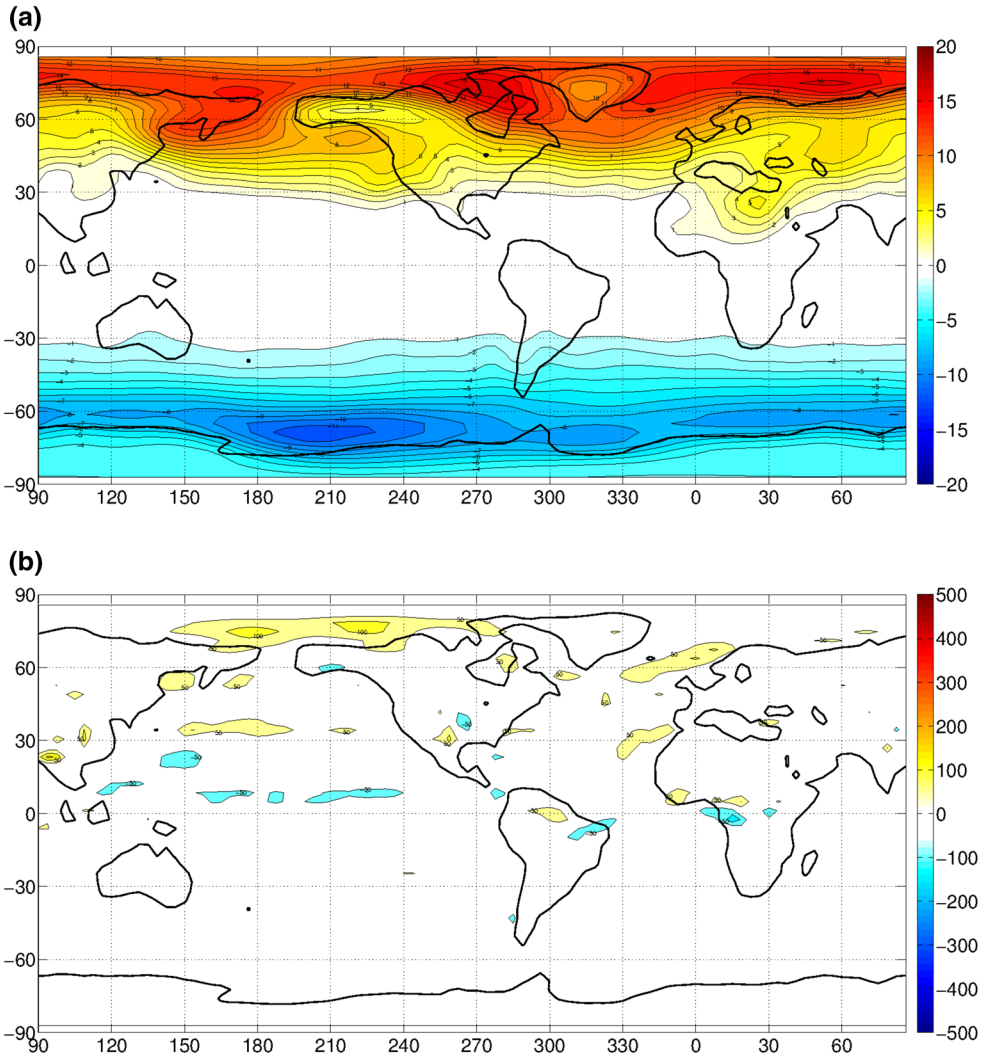

Fig. 16 Same as Fig. 3 for the experiment with fixed tropical SST, global slab land and fixed clear-sky longwave radiation *fix_trop_SST_fix_cslw_35* except that the control run is the one corresponding to this experiment setup

hemisphere. Transports performed by the mean circulation respond to the forcing with an intensification (weakening) of the southern (northern) Hadley and, to a lesser extent, Ferrel cells in the SH (NH). Meanwhile the changes in the fraction of the transport performed by transient eddies are found to be stronger in the SH, where they drive a poleward intensification of the zonal flow in the SH. An integration of the former leads to a net meridional atmospheric transport increased (decreased) to the SH (NH) and a consequent displacement of the energy equator towards the warmer hemisphere.

In the simulations in which the slab land model is applied globally but in the ocean the tropical SSTs are not allowed to change we found that the ITCZ response notably weakens. However, there is still some non negligible ITCZ response in particular over the Atlantic Ocean and Africa. In these regions the magnitude of the precipitation anomalies is of the order of 20 and 60 %, respectively, of that obtained when the tropical SST constraint was not applied. Cvijanovic and Chiang (2013) performed a similar experiment and also found that by disabling the tropical SST reaction the ITCZ response almost disappears, although in their results significant tropical precipitation changes were essentially not present in any location. This discrepancy in the ITCZ response could be caused by the use of different AGCMs. Based on our results the tropical SSTs are extremely important but not necessary in order to obtain a shift of the ITCZ to the warmer hemisphere, in particular over the Atlantic Ocean and Africa. With respect to atmospheric transports, as a direct consequence of the stillness of the tropical SSTs, the mean meridional circulation shows almost no response in the tropical region while the effect over the Ferrel cells and the transports performed by eddies is similar to the obtained without the

SST constraint. Regarding the physical mechanism we hypothesize that, in the absence of an inter-hemispheric SST gradient in the tropical region, the continental surface temperature over Africa is the one responsible for the ITCZ displacements.

With this motivation in mind we performed the third set of simulations in which fixed surface temperatures over Africa are imposed as an additional constraint. In this case we found that the ITCZ response completely vanishes, indicating that the ITCZ response to the extratropical forcing is not possible just trough purely atmospheric processes, but needs the involvement of either the tropical SST or the continental surface temperatures. An additional experiment showed that an enhancement of the clear-sky longwave greenhouse effect plays a fundamental role in the warming over northern Africa. The warming is associated with a local decrease in sea level pressure that drives the ITCZ shift.

It is worth noting that the relevance of the surface air temperature over the Sahara desert as a driver of the Sahel rainfall variability has been previously highlighted, both in observations and model simulations by Haarsma et al. (2005).

Further work is planned in order to understand the role of the tropical ocean dynamics in the communication of the extratropical signal to the tropical region.

Acknowledgments Part of this work was performed while the first author was supported by Grants from Universidad de la República and Agencia Nacional de Investigación e Innovación (ANII), Uruguay.

References

Barreiro M, Philander SG (2008) Response of the tropical Pacific to changes in extratropical clouds. Clim Dyn 31:713–729. doi:10.1007/s00382-007-0363-5

Barreiro M, Fedorov A, Pacanowski R, Philander SG (2008) Abrupt climate changes: how freshening of the northern Atlantic affects the thermohaline and wind-driven oceanic circulations. Annu Rev Earth Planet Sci 36:33–58

Boccaletti G, Pacanowsk RC, Philander SG, Fedorov A (2004) The thermal structure of the upper ocean. J Phys Oceanogr 34:888–902. doi:10.1175/2008MWR2277.1

Burls N, Fedorov A (2014) What controls the mean east–west sea surface temperature gradient in the equatorial Pacific: the role of cloud albedo. J Clim 27:2757–2778. doi:10.1175/JCLI-D-13-00255.1

Chiang JC, Bitz CM (2005) Influence of high latitude ice cover on the marine Intertropical Convergence Zone. Clim Dyn 25:477–496. doi:10.1007/s00382-005-0040-5

Chiang JC, Friedman AR (2012) Extratropical cooling, interhemispheric thermal gradients, and tropical climate change. Annu Rev Earth Planet Sci 40:383–412. doi:10.1146/annurev-earth-042711-105545

Cvijanovic I, Chiang JC (2013) Global energy budget changes to high latitude North Atlantic cooling and the tropical ITCZ response. Clim Dyn 40:1435–1452. doi:10.1007/s00382-012-1482-1

Folland CK, Palmer TN, Parker DE (1986) Sahel rainfall and worldwide sea temperatures, 1901–85. Nature 320:602–607. doi:10.1038/320602a0

Giannini A, Saravanan R, Chang P (2003) oceanic forcing of Sahel rainfall on interannual to interdecadal time scales. Science 7:1027–1030. doi:10.1126/science.1089357

Gu DG, Philander SG (1997) Interdecadal climate fluctuations that depend on exchanges between the tropics and extratropics. Sci 275:805–807

Haarsma RJ, Selten FM, Weber SL, Kliphuis M (2005) Sahel rainfall variability and response to greenhouse warming. Geophys Res Lett 32:L17702

Hartmann DL (1994) Global physical climatology. International Geophysics Series, vol 56. Academic Press, San Diego, USA

Holton JR (2004) An introduction to dynamic meteorology, 4th edn. International Geophysics Series, vol 88. Academic Press, New York, USA

Hughen KA, Southon JR, Lehman SJ, Overpeck JT (2000) Synchronous radiocarbon and climate shifts during the last deglaciation. Science 290:1951–1954

Kalnay E et al (2006) The NCEP/NCAR 40-year reanalysis project. Bull Am Meteorol Soc 77:437–470

Kang SM, Held IM, Frierson DM, Zhao M (2008) The response of the ITCZ to extratropical thermal forcing: idealized slab-ocean experiments with a GCM. J Clim 21:3521–3532. doi:10.1175/2007JCLI2146.1

Kang SM, Frierson DM, Held IM (2009) The tropical response to extratropical thermal forcing in an idealized GCM: the importance of radiative feedbacks and convective parameterization. J Atmos Sci 66:2812–2827. doi:10.1175/2009JAS2924.1

Kucharski F, Molteni F, Bracco A (2006) Decadal interactions between the western tropical Pacific and the North Atlantic Oscillation. Clim Dyn 26:79–91. doi:10.1007/s00382-005-0085-5

Lin J-L (2007) The double-ITCZ problem in IPCC AR4 coupled GCMs: ocean-atmosphere feedback analysis. J Clim 20:4497–4525. doi:10.1175/JCLI4272.1

Liu Z, Yang H (2003) Extratropical control of tropical climate, the atmospheric bridge and oceanic tunnel. Geophys Res Lett. doi:10.1029/2002GL016492

Liu Y, Guo L, Wu G, Wang Z (2010) Sensitivity of ITCZ configuration to cumulus convective parameterizations on an aqua planet. Clim Dyn 34:223–240. doi:10.1007/s00382-009-0652-2

Lorenz DJ, Hartmann DL (2001) Eddy-zonal flow feedback in the southern hemisphere. J Atmos Sci 58:3312–3327

Lynch-Stieglitz J (2004) Hemispheric asynchrony of abrupt climate change. Science 304:1919–1920

Manabe S, Stouffer RJ (1995) Simulation of abrupt climate change induced by freshwater input to the North Atlantic ocean. Nature 378:165–167

Molteni F (2003) Atmospheric simulations using a GCM with simplified physical parametrizations. I. Model climatology and variability in multi-decadal experiments. Clim Dyn 20:175–191

Peterson LC, Haug GH, Hughen KA, Rohl U (2000) Rapid changes in the hydrologic cycle of the tropical Atlantic during the last glacial. Science 290:1947–1951

Rahmstorf S (1995) Bifurcation of the Atlantic thermohaline circulation in response to changes in the hydrological cycle. Nature 378:145–149

Schneider T, Bischoff T, Haug GH (2014) Migrations and dynamics of the intertropical convergence zone. Nature 513:45–53

Song X, Zhang GJ (2009) Convection parameterization, tropical Pacific double ITCZ, and upper-ocean biases in the NCAR CCSM3. Part I: climatology and atmospheric feedback. J Clim 22:4299–4315. doi:10.1175/2009JCLI2642.1

Stouffer RJ et al (2006) Investigating the causes of the response of the thermohaline circulation to past and future climate changes. J Clim 19:698–722

Sun D-Z, Zhang T, Shin S-I (2004) The effect of subtropical cooling on the amplitude of ENSO: a numerical study. J Clim 17:3786–3798

Uppala SM et al (2005) The ERA-40 re-analysis. Q J R Meteorol Soc 131:2961–3012. doi:10.1256/qj.04.176

Vellinga M, Woods RA (2002) Global climatic impacts of a collapse of the Atlantic thermohaline circulation. Clim Chang 54:251–267

Wang X, Auler A, Edwards RL, Cheng H, Cristalli PS, Smart PL, Richards DA, Shen C (2004) Wet periods in northeastern Brazil over the past 210kyr linked to distant climate anomalies. Nature 432:740–743. doi:10.1038/nature03067

Yang H, Liu Z (2005) Tropical–extratropical climate interaction as revealed in idealized coupled climate model experiments. Clim Dyn 24:863–879. doi:10.1007/s00382-005-0021-8